Laser-induced periodic alignment of Ag nanoparticles in soda-lime glass

François Goutaland, Jean-Philippe Colombier, Mohamed Cherif Sow, Nadège Ollier, Francis Vocanson

Laser-induced periodic alignment of Ag nanoparticles in soda-lime glass

François Goutaland,[1*] Jean-Philippe Colombier,[1] Mohamed Cherif Sow,[1, 2] Nadège Ollier,[1] and Francis Vocanson[1]

[1]*Laboratoire Hubert Curien (UMR 5516 CNRS), Université de Lyon, Université de Saint-Etienne, 42000 Saint Étienne, France*

[2]*present address: Laboratoire LESI, 21 Rue de Loigny la Bataille, 28000 Chartres, France*

[*]*francois.goutaland@univ-st-etienne.fr*

Abstract: One-, two- or three-dimensional arrays of closely spaced silver nanoparticles may lead to new optical properties, due to short or long range coupling between their resonant surface plasmons, so that the spatially controlled growth of silver nanoparticles provides an efficient way to tune their optical properties. Towards this way, we present here the periodic pattern of a glass surface with silver nanoparticles by continuous ultraviolet laser exposure. The formation of the 160 nm period pattern is well described by an interference-based model which agrees with the experimental conclusions, mainly obtained by various forms of microscopy. Statistical approach based on the autocorrelation function gives quantitative description about the quality of the order in the periodic structure and about the nanoparticles averaged diameter (80 nm). We also present the optical extinction spectrum of the Laser Induced Periodic Surface Structure (LIPSS)-containing area of the glass, which unusually shows several bands in the visible range. The period of 160 nm of the periodic structure is short enough to allow coupling between nanoparticles, which makes it a possible candidate for plasmon-based optical applications.

OCIS codes: (140.3390) Laser materials processing; (220.4241) Nanostructure fabrication; (160.4236) Nanomaterials.

References and links

1. R. V. Ramaswamy and R. V. R. Srivastava, "Ion-exchanged glass waveguides: a review," J. Lightwave Technol. **6**(6), 984–1000 (1988).
2. M. Falconieri, G. Salvetti, E. Cattaruzza, F. Gonella, G. Mattei, P. Mazzoldi, M. Piovesan, G. Battaglin, and R. Polloni, "Large third-order optical nonlinearity of nanocluster-doped glass formed by ion implantation of copper and nickel in silica," Appl. Phys. Lett. **73**(3), 288–290 (1998).
3. N. Félidj, J. Aubard, G. Lévi, J. R. Krenn, M. Salerno, G. Schider, B. Lamprecht, A. Leitner, and F. R. Aussenegg, "Controlling the optical response of regular arrays of gold particles for surface-enhanced Raman scattering," Phys. Rev. B **65**(7), 075419 (2002).
4. K.-J. Berg, A. Berger, and H. Hofmeister, "Small silver nanoparticles in glass surface layers produced by silver-sodium ion exchange—their concentration and size depth profiles," Z. Phys. D **20**(1-4), 309–311 (1991).
5. F. Caccavale, G. De Marchi, F. Gonella, P. Mazzoldi, C. Meneghini, A. Quaranta, G. W. Arnold, G. Battaglin, and G. Mattei, "Irradiation-induced Ag-colloid formation in ion-exchanged soda-lime glass," Nucl. Instrum. Methods Phys. Res. B **96**, 382–386 (1995).
6. J. P. Blondeau, S. Pellerin, V. Vial, K. Dzierzega, N. Pellerin, and C. Andreazza-Vignolle, "Influence of pulsed laser irradiation on precipitation of silver nanoparticles in glass," J. Cryst. Growth **311**(1), 172–184 (2008).
7. F. Goutaland, E. Marin, J. Y. Michalon, and A. Boukenter, "Growth of silver nanoparticles of variable and controlled diameter in silica-based and soda-lime glasses by simultaneous continuous ultraviolet irradiation and heat treatment," Appl. Phys. Lett. **94**(18), 181108 (2009).
8. A. Toma, D. Chiappe, D. Massabo, C. Boragno, and F. Buatier de Mongeot, "Self-organized metal nanowire arrays with tunable optical anisotropy," Appl. Phys. Lett. **93**(16), 163104 (2008).
9. G. Seifert, M. Kaempfe, F. Syrowatka, C. Harnagea, D. Hesse, and H. Graener, "Self-organized structure formation on the bottom of femtosecond laser ablation craters in glass," Appl. Phys., A Mater. Sci. Process. **81**(4), 799–803 (2005).
10. M. Ranjan, T. W. H. Oates, S. Facsko, and W. Möller, "Optical properties of silver nanowire arrays with 35 nm periodicity," Opt. Lett. **35**(15), 2576–2578 (2010).

#197893 - $15.00 USD Received 17 Sep 2013; revised 6 Nov 2013; accepted 11 Nov 2013; published 16 Dec 2013

11. H. S. Won and S. H. Song, "Metallic nanocluster gratings generated by near-field coupling of localized surface plasmons," Opt. Express **14**(24), 11814–11822 (2006).
12. K. Kaneko, H.-B. Sun, X.-M. Duan, and S. Kawata, "Two-photon photoreduction of metallic nanoparticle gratings in a polymer matrix," Appl. Phys. Lett. **83**(7), 1426–1429 (2003).
13. K. Loeschner, G. Seifert, and A. Heilmann, "Self-organized, gratinglike nanostructures in polymer films with embedded metal nanoparticles induced by femtosecond laser irradiation," J. Appl. Phys. **108**(7), 073114 (2010).
14. F. Goutaland, M. Sow, N. Ollier, and F. Vocanson, "Growth of highly concentrated silver nanoparticles and nanoholes in silver-exchanged glass by ultraviolet continuous wave laser exposure," Opt. Mater. Express **2**(4), 350–357 (2012).
15. J. E. Sipe, J. F. Young, J. S. Preston, and H. M. van Driel, "Laser-induced periodic surface structure. I. Theory," Phys. Rev. B **27**(2), 1141–1154 (1983).
16. S. Malynych and G. Chumanov, "Light-Induced Coherent Interactions between Silver Nanoparticles in Two-Dimensional Arrays," J. Am. Chem. Soc. **125**(10), 2896–2898 (2003).
17. R. J. Nemanich, D. K. Biegelsen, and W. G. Hawkins, "Aligned, coexisting liquid and solid regions in laser-annealed Si," Phys. Rev. B **27**(12), 7817–7819 (1983).
18. M. Birnbaum, "Semiconductor surface damage produced by ruby lasers," J. Appl. Phys. **36**(11), 3688–3689 (1965).
19. J. F. Young, J. E. Sipe, J. S. Preston, and H. M. Van Driel, "Laser-induced periodic surface damage and radiation remnants," Appl. Phys. Lett. **41**(3), 261–264 (1982).
20. R. M. Osgood, Jr. and D. J. Ehrlich, "Optically induced microstructures in laser-photodeposited metal films," Opt. Lett. **7**(8), 385–387 (1982).
21. F. Garrelie, J. P. Colombier, F. Pigeon, S. Tonchev, N. Faure, M. Bounhalli, S. Reynaud, and O. Parriaux, "Evidence of surface plasmon resonance in ultrafast laser-induced ripples," Opt. Express **19**(10), 9035–9043 (2011).
22. A. E. Siegman and P. M. Fauchet, "Stimulated Wood's anomalies on laser-illuminated surfaces," IEEE J. Quantum Electron. **22**(8), 1384–1403 (1986).
23. H. M. Van Driel, J. E. Sipe, and J. F. Young, "Laser-Induced Periodic Surface Structure on Solids: A Universal Phenomenon," Phys. Rev. Lett. **49**, 1955–1958 (1982).
24. I. Antonov, F. Bass, Y. Kaganovskii, M. Rosenbluh, and A. Lipovskii, "Fabrication of microlenses in Ag-doped glasses by a focused continuous wave laser beam," J. Appl. Phys. **93**(5), 2343–2348 (2003).
25. M. D. Niry, J. Mostafavi-Amjad, H. R. Khalesifard, A. Ahangary, and Y. Azizian-Kalandaragh, "Formation of silver nanoparticles inside a soda-lime glass matrix in the presence of a high intensity Ar+ laser beam," J. Appl. Phys. **111**(3), 033111 (2012).
26. A. Miotello, M. Bonelli, G. D. Marchi, G. Mattei, P. Mazzoldi, C. Sada, and F. Gonella, "Formation of silver nanoclusters by excimer–laser interaction in silver-exchanged soda-lime glass," Appl. Phys. Lett. **79**(15), 2456–2458 (2001).

1. Introduction

Soda-lime glasses doped with silver ions by the ion exchange technique were initially employed in the production of active or passive waveguiding systems [1]. Doping these glasses with embedded silver nanoparticles broadens their potential applications, as shown by the experimental demonstrations of all-optical switching [2] or molecular detection through Surface Enhanced Raman Scattering (SERS) [3]. The optical properties of these composite glasses are mainly dominated by the Surface Plasmon Resonance (SPR) of the silver nanoparticles, responsible for an absorption band in the visible range, whose spectral position is affected by the surrounding dielectric matrix, the morphology (size and shape) and the spatial organization of the nanoparticles. Such composite glasses are usually fabricated by several experimental ways, using a silver-exchanged soda-lime glass as starting material, submitted to various treatments to promote the formation of silver nanoparticles of controlled shape and size: thermal annealing into hydrogen atmosphere [4], ion irradiation [5] or irradiation by either pulsed or continuous wave (cw) laser exposure [6, 7]. However, spatial ordering of the silver nanoparticles, which confers new optical properties to the composite glass [8–10], cannot be carried out by any of these techniques. It can be achieved by laser irradiation, through an interference pattern, of period of few micrometers, due to the coherent interference between two laser beams, of a composite soda-lime glass containing silver nanoparticles [11]. The resulting metallic grating of 3.5 μm period, consists of a periodic arrangement of silver nanoparticles of 100 nm diameter located in the dark fringes of the interference pattern. Much smaller period of few hundreds of nanometers has been reported in a polymer dielectric matrix doped with silver ions or nanoparticles, submitted to femtosecond exposure [12, 13]. In this case, self-organization among silver nanoparticles is responsible for their periodic distribution and is associated to the growth of Laser Iinduced Periodic Surface

#197893 - $15.00 USD Received 17 Sep 2013; revised 6 Nov 2013; accepted 11 Nov 2013; published 16 Dec 2013

Structure (LIPPS), which results from the interference between the incident laser beam and backscattered surface waves. In this paper, we demonstrate that the LIPSS, which growths during continuous wave (cw) ultraviolet (UV) laser exposure of a silver-exchanged glass, consists of a periodic arrangement between silver nanoparticles. The regular arrangement is composed by isolated silver nanoparticles of 80 nm in diameter, separated by about 20 nm and aligned along lines periodically spaced by 160 nm, as shown by Scanning Electron Microscopy (SEM) and Atomic Force Microscopy (AFM) characterizations. It is worth to notice that we merely mentioned the presence of periodically organized silver nanoparticles in a previous paper [14]. We report very good agreement between the measured and calculated periods of the arrangement, determined by the first-principle theory developed by Sipe et al. [15]. The nanoparticles alignment, parallel to the laser polarization, is also consistent with energy distribution predicted by the model of Sipe. Besides nanoparticles organization analyzed by statistical correlations, we show that the absorption spectrum measured across the periodic arrangement exhibits several narrow absorption bands, due to the SPR of the silver nanoparticles in the visible range. Therefore, regular organization between silver offers the ability to originate additional resonance bands. Finally, we propose that the formation of the periodic arrangement is due to the diffusion of silver nanoparticles from the depth of the exchanged layer towards its surface, transversally modulated by the light intensity distribution.

2. Experimental procedure

The LIPSS are produced on silver-exchanged soda-lime glasses by intense cw laser exposure at 244 nm. Commercial glass slides have been used in which silver ions have been incorporated by the ion exchange technique [14]. LIPSS are formed by focusing the laser on the glass surface by using a x10 microscope objective, with a power density of about 1200 kW/cm^2. Laser spots have been written at the glass surface for different exposure times from 500 ms to 5s, by use of an optical shutter. No surface damages have been observed except for exposure times higher than 5s. The LIPSS formed within the laser spots have been characterized by optical microscopy, SEM and AFM. The absorption spectrum of the LIPSS containing area has been measured with a confocal spectrometer used in the transmission mode and equipped with a UV/visible source, with a high spatial resolution of few micrometers.

3. Results

Figure 1(a) displays a SEM picture of a laser spot inscribed at the glass surface irradiated for 500 ms. The formation of large nanoparticles (roughly 125 nm in diameter) in the outer regions of the laser spot has been previously explained [10], where the major role played by the very large temperature rise is addressed. Due to the locally high absorption of the laser beam by the glassy matrix, the glass is heated to a temperature higher than the glass transition temperature, which results into the formation of glass droplets, whose shape is maintained after rapid cooling due to the end of the exposure [14]. The glass surface contains thus bumps of few hundred of nanometers height after the laser exposure. Silver nanoparticles, which are formed below the surface exposed to the laser irradiation within the first 200 μs of the laser exposure, move in the molten glass temperature gradient towards the periphery of the glass drops, where they coalesce into larger nanoparticles [14].

#197893 - $15.00 USD Received 17 Sep 2013; revised 6 Nov 2013; accepted 11 Nov 2013; published 16 Dec 2013

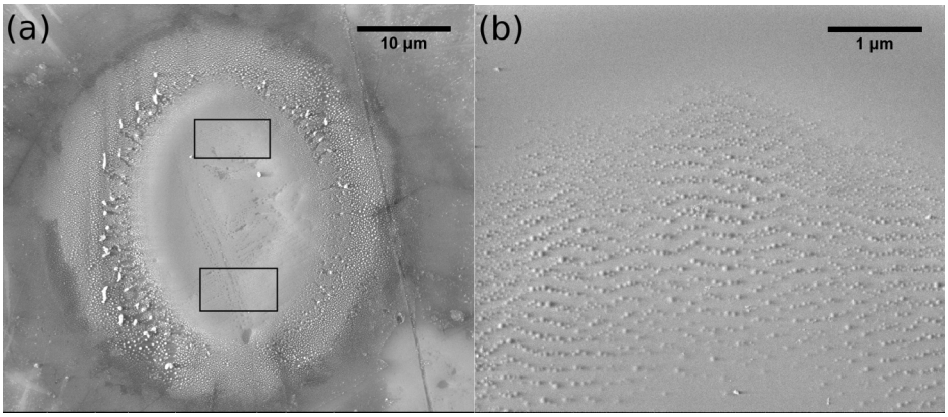

Fig. 1. (a): SEM image of a laser spot inscribed during 500 ms; (b): zoom within the LIPPS containing area.

Looking with more details to the circled areas in Fig. 1(a) reveals periodic waves at the glass surface. These waves consist of organized nanoparticles, of diameter ranging between 50 and 100 nm, with a period of roughly 160 nm [Fig. 1(b)]. These nanoparticles are aligned across waves of about 2 µm length and are mostly formed near the two vertical poles of the laser spot. It is worth to mention that the orientation of these LIPSS was found to be parallel to the laser polarization, which means that their wave vector is perpendicular to the laser polarization. The periodic arrangement between nanoparticles becomes slightly more obvious for an exposure of 1s [Fig. 2(a)] and is much more clearly revealed in case of an exposure time of 3s [Fig. 2(b)]: the nanoparticles are aligned along lines of 2 to 3 µm length spaced by 160 nm and are distributed within a ring of few micrometers thickness surrounding the laser spot. Their diameter is estimated at 80 nm distributed over a rather narrow distribution, and the regularity of the periodic arrangement becomes higher.

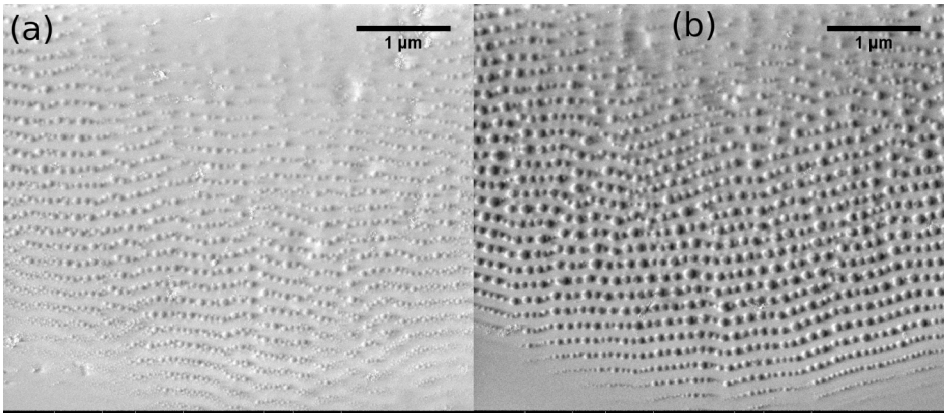

Fig. 2. (a): SEM image of the periodic arrangement between silver nanoparticles observed after an irradiation time of 1s; (b): SEM image of the periodic arrangement between silver nanoparticles observed after an irradiation time of 3s.

To give more quantitative evidence to these observations, we have performed the calculation of the radially averaged autocorrelation function, as shown in Fig. 3.

#197893 - $15.00 USD Received 17 Sep 2013; revised 6 Nov 2013; accepted 11 Nov 2013; published 16 Dec 2013

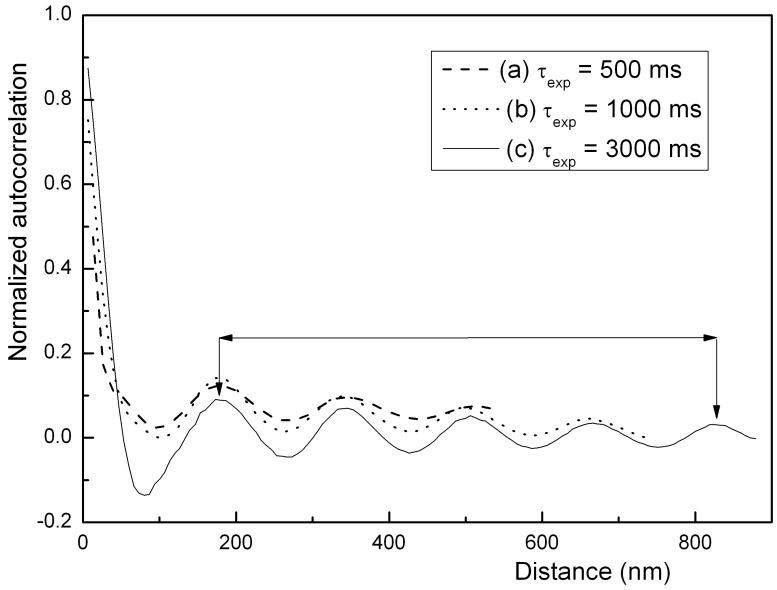

Fig. 3. curves of the autocorrelation function calculated from the SEM images: curve (a) corresponds to Fig. 1(b), curve (b) to Fig. 2(a) and curve (c) to Fig. 2(b).

The radially averaged autocorrelation is calculated from the autocorrelation (also known as pair correlation) of pixels of a binary image as a function of their radial distance. The oscillating behavior of the curves obtained for three different exposure times is clear evidence for long-range order (curves (a), (b) and (c) in Fig. 3). The first minimum of this function gives information on the particle size, while the period of the arrangement is averaged over several maxima of the curve. We have estimated the diameter of the nanoparticles to 78 nm for the longer exposure time, and to 90 nm for the two lowest exposure times. However, this latter value, which does not precisely match with the corresponding SEM pictures [Fig. 1(b) and Fig. 2(a)], is much more uncertain since the first minima in curve (a) and curve (c) is not well-defined (a shoulder can be observed located at around 40 nm), due to the lower regularity of the periodic arrangement. The period between the lines along which the nanoparticles are aligned is equal to 160 nm for the three different exposure times, in good agreement with the period estimated from the SEM images [Fig. 1(b), 2(a) and 2(b)]. The long-ranged order is maintained over more than 1 μm in case of the longest laser exposure time, while it is reduced to about 700 nm in case of the shorter exposure times. The oscillating behavior of curve (a) in Fig. 3 gives evidence of the regularity of the arrangement between nanoparticles for the shortest exposure time, which is not so obvious in the SEM image [Fig. 1(b)]. It is worth to notice that no significant evolution of the statistical properties of the arrangement is observed for exposure times larger than 3s, neither for the particles spacing nor for the particles diameter.

#197893 - $15.00 USD Received 17 Sep 2013; revised 6 Nov 2013; accepted 11 Nov 2013; published 16 Dec 2013

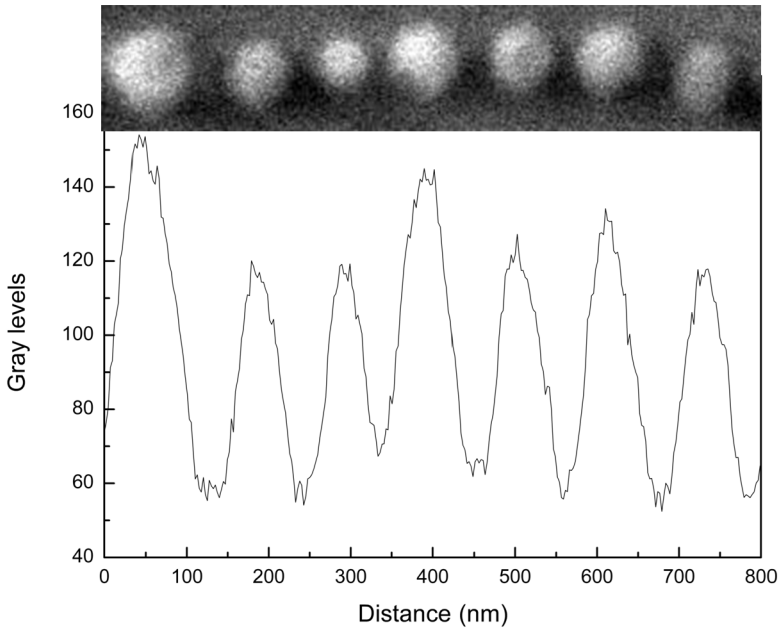

Fig. 4. surface profile plot, extracted along the line shown in the inset of the graph, showing the regularity of the silver nanoparticles alignment.

The nanoparticles distributed along a line are periodically spaced from center to center for about 100 nm, as shown by Fig. 4, which displays the surface profile plot, extracted from the SEM image depicted in Fig. 2(b). Therefore, the edge to edge distance between two consecutive nanoparticles is estimated at around 20 nm. A silver nanoparticle of diameter 50 nm only and therefore much smaller than the averaged diameter of 80 nm, is clearly observed in the inset of Fig. 4 (third form the left position). The statistical analysis based on the averaged autocorrelation function [Fig. 3] gives evidence that this smaller diameter remains an exception in the nanoparticles size distribution. The periodicity along the lines should be reflected in the curves of the radially averaged autocorrelation function but is not observed Fig. 3]. The most likely explanation is that the oscillating behavior of the curves in Fig. 3 is characteristic of the larger period (160 nm between the lines) only and hides the smaller one. The contrast between two consecutive nanoparticles along a line is smaller than that between the lines, which also favors the oscillations due to the larger period.

The SEM analysis does not give any information about the composition of the aligned nanoparticles, which thus remains unknown at this point of the paper, even if our previous report [14] strongly suggests that the aligned nanoparticles are silver nanoparticles. One simple way to investigate the composition of the nanoparticles is to measure the absorption spectrum to check whether the absorption band due to the surface plasmon resonance band of silver nanoparticles is observed or not. Figure 5(b) displays the absorption spectrum recorded across two different zones around the laser spot, shown in Fig. 5(a). Due to the 12µm spatial resolution of the absorption measurements, overlapping between the two different areas occurs, so that the absorption bands depicted in Fig. 5(b) do not come solely from zones 1 or 2. The band centered at 445 nm, recorded across the outer regions [area 2, red curve], is ascribed to the SPR of silver nanoparticles, according to its width and spectral position [14]. This band is also observed in the absorption spectrum recorded from the region which contains the periodic arrangement of nanoparticles [area 1, black curve], evidencing that the aligned nanoparticles are silver nanoparticles. The black curve exhibits three narrower bands centered at 510, 600 and 730 nm, whose presence is most likely due to the influence of the periodic arrangement between silver nanoparticles [16]. Due to the short distances between

#197893 - $15.00 USD Received 17 Sep 2013; revised 6 Nov 2013; accepted 11 Nov 2013; published 16 Dec 2013

the aligned nanoparticles, coupling between the local fields from individual nanoparticles is expected, which can lead to different sharp bands in the absorption spectrum due to SPR of silver nanoparticles [16], depending on the number of nanoparticles involved in the plasmon interaction [16]. The investigation of the exact mechanism is far beyond the scope of this paper and requires further diagnostics. It is worth to notice that we have observed, by SEM analysis (not depicted in this paper), a similar periodic arrangement between nanoparticles, after having laser-processed a similar glass sample doped with gold ions. In this case, the absorption spectrum recorded across the periodic arrangement exhibits absorption bands characteristic of the SPR of gold nanoparticles. This experimental observation reinforces the assumption that the aligned nanoparticles are metallic nanoparticles.

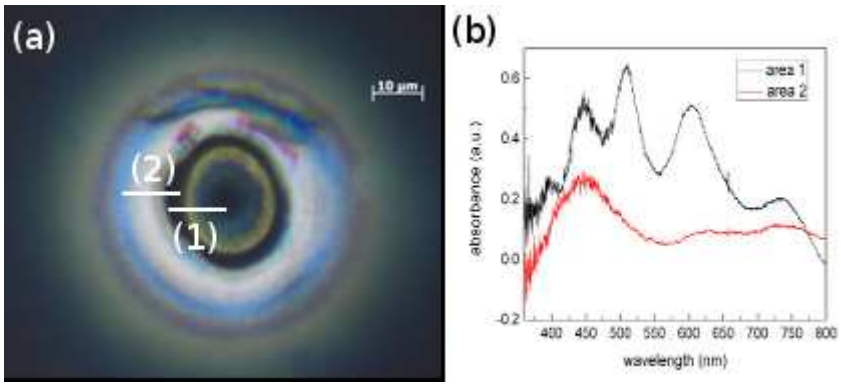

Fig. 5. (a): optical microscope image (reflexion mode) showing the position and length of the two different areas across which the absorption spectra depicted in Fig. 5(b) have been recorded: area (1): region containing the periodic alignment of silver nanoparticles; area (2): outer region which contain large silver nanoparticles; (b): absorption spectra of areas 1 and 2 .

Before discussing the mechanism explaining the formation of the aligned nanoparticles, we will address the question of whether the contrast in the SEM pictures is due to differences in the material composition only or if a topological effect contributes also to this contrast. We have performed AFM analysis of the area containing the aligned nanoparticles to answer this question.

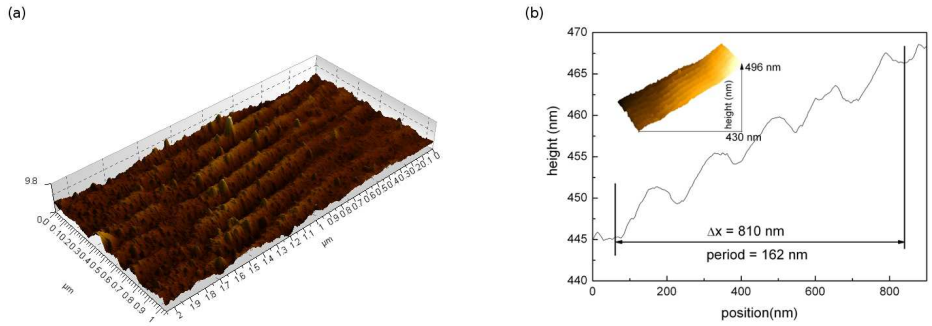

Fig. 6. (a): 3D AFM image corrected from the slope of the glass droplet; (b): height profile extracted absorption along the black line shown in the inset (AFM image showing the LIPSS superimposed on the glass droplet)

Figure 6(a) shows the surface modulation due to the formation of LIPSS, superimposed on the curvature of the glass droplet. It is worth to notice that the aligned nanoparticles do not appear (are not clearly resolved) clearly in the AFM image, instead continuous lines are observed. Taking into account their spacing of about 20 nm along the lines, the silver nanoparticles should be resolved in the AFM image according to the lateral resolution of the microscope of about 4 nm. The lack of well-resolved nanoparticles in the AFM image is

#197893 - $15.00 USD Received 17 Sep 2013; revised 6 Nov 2013; accepted 11 Nov 2013; published 16 Dec 2013

explained by the almost complete burial of the nanoparticles below the glass surface, as shown by the height profile displayed in Fig. 6(b). This profile reveals that the height with which the nanoparticles emerge above the glass surface, lies between 2 and 4 nm, while the period between the lines is 162 nm, in good agreement with previous estimations. Therefore, the depth in between two consecutive nanoparticles is too small for the AFM tip to obtain a correct image. The inset of Fig. 6(b) shows a 3D AFM image, reconstructed from the AFM profile and corrected from the glass droplet slope, which confirms the high regularity of the periodic arrangement.

4. Discussion

As mentioned in the introduction of this paper, the Sipe's model [15] allows predicting the period of the LIPSS, as well as their orientation relative to the laser polarization direction, in various materials submitted to either cw or pulsed laser exposure [17–20]. Disagreements between this model and some experimental reports have been reported in case of fs-pulsed laser exposure, due to various effects of short time scale [21]. This model is based on the interference between an incident laser beam with some scattered electromagnetic waves due to surface roughness, which leads to the periodic modulation of the laser electric field. It predicts for which Fourier components k the rough surface can concentrate the incident energy, as a function of the laser exposure parameters (angle of incidence θ, polarization direction, and wave vector of the incident radiation which has a component $\mathbf{k_i}$ in the surface plane) and on the surface parameters (optical index and surface roughness). Figure 7(a) shows the irradiation geometry. The material surface roughness is decomposed into Fourier series over spatial frequencies corresponding to different wave vectors. The inhomogeneous energy deposition I(**k**), due to the interferences between incident and diffracted fields, is written according to Eq. (1):

$$I(k) \propto \eta(k, ki)\,|b(k)| \tag{1}$$

with **k** a wave vector parallel to the surface, normalized to the incident laser wave vector, η(**k**, $\mathbf{k_i}$) the scalar efficacy with which the surface roughness at **k** leads to inhomogeneous absorption of the laser and b(**k**) the surface roughness amplitude. The main assumption is that LIPSS grow where the deposited energy is the largest. This energy is related to the efficacy factor η, which is convenient to have a synthetic representation of the complex radiative and non-radiative field structures at the surface [15]. The efficacy factor contains sharp peaks at certain values **k**, which are usually superimposed on a slowly varying background. In a semiquantitative comparison, these peaks can be associated with the LIPSS and provides an estimation of their spatial period Λ, which can be derived from the equation $\Lambda = \lambda\,[n(1 \pm \sin\theta)]^{-1}$, where λ is the laser wavelength and n the refractive index [22].

We have calculated numerically η(**k**, $\mathbf{k_i}$), as a function of the normalized LIPSS wave vectors $\mathbf{k_x}$ and $\mathbf{k_y}$ ($|k| = 2\pi/\lambda$), whose map reveals a sharp peak, which corresponds to LIPSS parallel to the laser polarization for $\Lambda \approx \lambda/n$, as expected for low-index dielectric materials [Fig. 7(b)]. This calculation has been performed for the laser experimental parameters ($\theta = 0°$ and $\lambda = 244$ nm) and for parameters characterizing the bulk optical properties (the complex dielectric permittivity $(n + ik)^2$, with n and k being the refractive index and the extinction respectively) and the surface roughness properties (s, f). These two latter parameters represent the shape factor and the filling factor of the selvedge region between the air and the bulk material and have been chosen equal to 0.4 and 0.1 respectively, with the assumptions of isolated spherical islands [23]. η is almost independent of these surface parameters, yielding the model free of adjustable parameters. We have estimated the absorbance of the glass to 4, by polishing the commercial glass slide to a thickness of 135 μm. The absorption coefficient α of the glass is given by $\alpha = -1/135 \times \ln(10^{-4}) = 6.82 \times 10^{-2}\ \mu m^{-1}$. This leads to an extinction coefficient k given by: $k = \alpha\lambda/4\pi \cong 1.32 \times 10^{-3}$. Concerning the value of the refractive index of the Ag^+-exchanged glass, M-Lines measurements indicate that the refractive index is about 1.6 at the glass surface and decreases rapidly with an almost

#197893 - $15.00 USD Received 17 Sep 2013; revised 6 Nov 2013; accepted 11 Nov 2013; published 16 Dec 2013

parabolic profile down to the value of 1.51 typical of the virgin glass, within the first 5 to 6 µm of the exchanged layer. The irradiated layer consists in a glassy matrix, doped with Ag^+ ions, presenting a parabolic refractive index profile, where the laser penetration depth can be estimated to be around 10 µm. The transient value of the optical properties in the laser absorption zone exhibiting such inhomogeneity has not been clearly established. We have previously shown that silver is driven out the laser exposed area within the first few µs of the laser exposure and consequently the refractive index within the area modified by the laser exposure is thus expected to rapidly decrease, due to the lack of silver. Since the LIPSS formation appears after an exposure time of at least 500 ms, we have chosen a refractive index value of 1.51, corresponding to that glass free of silver near the surface.

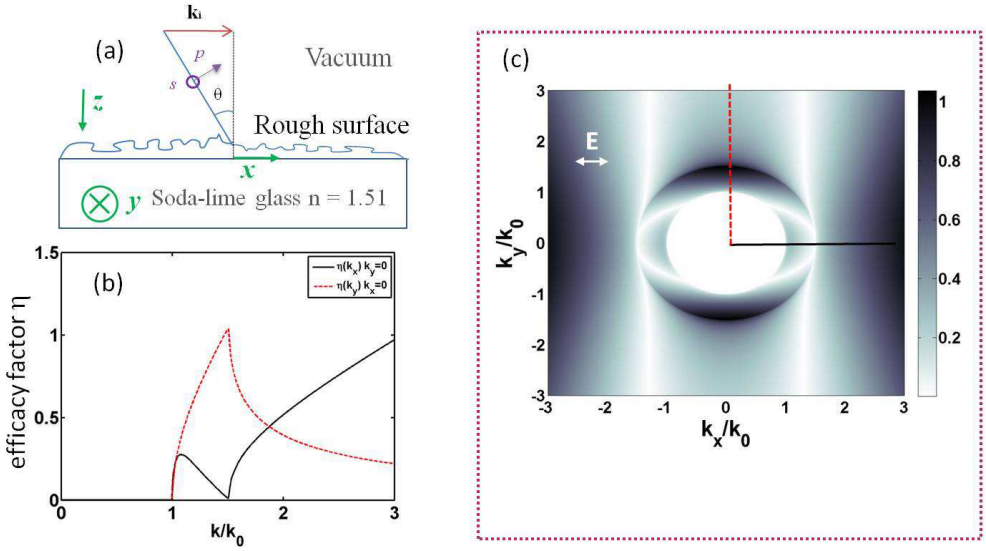

Fig. 7. (a): Geometry of the laser beam incidence to a rough surface, used to model the growth of LIPSS; (b): curve of the efficacy factor η versus the normalized wave vectors k_x and k_y. The maximum of the curve shows that LIPSS growth in the y direction only and gives a period of 163 nm; (c): 2D gray scale map of the efficacy factor η as function of the normalized wave vectors k_x and k_y. The values of η are encoded in a gray scale with darker tints representing larger values.

We have then shown that Sipe's model predicts the existence of k values for which the light intensity at the sample surface exhibits maxima values. This leads to a LIPSS period of $\Lambda \cong 162$ nm, in very good agreement with the different experimental results obtained by SEM, AFM measurements as well as by the calculation from the autocorrelation function. Figure 7(c) shows a 2D gray scale map of the calculated efficacy factor η as a function of the normalized LIPSS wave vectors components k_x and k_y. The symmetric arrangement of the features located above and below the central part of the map, corresponds to LIPSS having lines parallel to the laser polarization and to a LIPSS period close to λ/n. During the steady-state development of periodic structures, the material remains polariton inactive media and no resonance is observed for wave vectors corresponding to coupling to surface plasmon polariton. To further characterize the periodic arrangement, the SEM pictures 1b and 2b have been submitted to a two-dimensional Fourier Transform (2D-FT), shown in Figs. 8(a) and 8(b). Sickle-shaped feature can be clearly seen in each case, which corresponds to period of 165 nm, in good agreement with the values predicted by the theory. The shape of this feature agrees well with that of the calculated feature observed in Fig. 7(c). The harmonics of the sickle-shape feature, which can be observed in the 2D-FT image calculated for the longer exposure time (3s), are characteristic of the long-range order of the arrangement. These

#197893 - $15.00 USD Received 17 Sep 2013; revised 6 Nov 2013; accepted 11 Nov 2013; published 16 Dec 2013

harmonics tend to disappear in case of the shorter exposure time, due to the less ordered pattern.

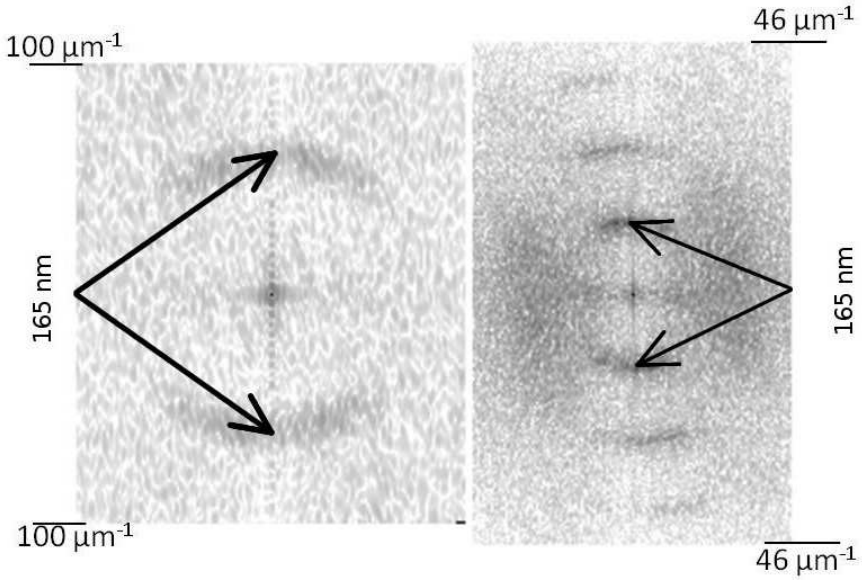

Fig. 8. (a): 2D FT of Fig. 1(b); (b): 2D FT of Fig. 2b. The sickle-shaped features, expected from the calculations displayed in Fig. 7(c), indicate a LIPSS period of about 165 nm in each case.

The comparison between experimental and theoretical results indicates undoubtedly that the formation of the periodic arrangement between silver nanoparticles obeys to the Sipe's model. Therefore, an interference pattern formed at the glass surface near the irradiated spot is involved in the alignment of the silver nanoparticles. We have previously demonstrated [14] that silver nanoparticles formed at the glass surface during the first few µs of the laser exposure, are embedded into a liquid glass phase and then pushed into the outer regions where the viscosity is lower than in the center of the spot. Previous reports have mentioned that the irradiated spots are free of silver nanoparticles in either Ag^{+}-doped glasses or in composite glasses containing silver nanoparticles after intense cw laser exposure at 244 nm or in the visible range [14, 24, 25]. It is thus likely that the silver nanoparticles involved in the periodic arrangement come from the depth of the exchanged layer, where the initial silver ions concentration is much lower than at the glass surface. Diffusion of the silver buried species (nanoparticles and ions) towards the glass surface, which has been reported under cw or pulsed laser exposure of a composite glass [24, 26] is required to explain the LIPSS formation. The higher solubility of the silver species in the liquid phase, located near the glass surface, than in the solid phase explains the diffusion process. Niry et al. [23] reported that diffusion does not take place at the beginning of the laser exposure but after a delay of one minute. This delay is much shorter (500 ms) in our case due to the much higher absorption of the laser wavelength. Silver species are thus floating within the liquid phase near the glass surface and forces due to surface tension prevent them to diffuse back towards the bulk glass. Accumulation of silver ions occurs and leads to their precipitation into nanoparticles, whose concentration is expected to be large at the glass surface, so that the irradiated surface exhibits a metallic character. LIPSS growth then takes place and leads to the regular organization between silver nanoparticles, according to the interference pattern. Silver nanoparticles, which are known to usually escape cw laser light when embedded in a glassy matrix [11], are thus most likely aligned within the dark fringes of this pattern. The dynamics of the resolidification, which occurs as soon as the laser exposure is stopped, plays a key role in the periodic organization of the silver nanoparticles, as it freezes their position in the dark fringes,

#197893 - $15.00 USD Received 17 Sep 2013; revised 6 Nov 2013; accepted 11 Nov 2013; published 16 Dec 2013

superimposed to the glass droplet. The freezing of these nanoparticles floating within the liquid phase explains as well their almost complete burial below the glass surface [Fig. 6]. LIPSS have not been observed in pure soda-lime, despite the formation of glass droplets, which gives evidence that large temperature increase has occurred to the laser exposure. Therefore, the presence of metal is required for the LIPSS to grow, which is confirmed by their observation in similar glass doped with gold nanoparticles. In this case, the period of the periodic structure and the size of the gold nanoparticles are identical to those measured for silver-doped samples, which indicates that the kind of metal involved does not play any role. This suggests that the plasmonic nature of the LIPSS growth [21] can be ruled out in our case, according to the theoretical calculations [Fig. 7(c)].

5. Conclusion

By combining the ion exchange technique with cw UV laser irradiation of a soda-lime glass, we have triggered the formation of periodic alignment of silver nanoparticles. Different microscopy characterizations reveal silver nanoparticles of diameter 80 nm are aligned along lines periodically spaced by 160 nm. Long-range order, over more than 1 μm, is clearly shown by SEM images and confirmed by the calculation of the radially averaged autocorrelation function. The model of Sipe, based on interference between the incoming laser beam and some form of a surface-scattered electromagnetic wave in the surface plane, seems to be reliable to explain the LIPSS. The regular organization between silver nanoparticles is explained by the growth of LIPSS around the laser spot after an irradiation time of about 500ms, necessary for the buried silver nanoparticles to reach the glass surface through a diffusion process. The interference pattern determines the position of these silver nanoparticles, which are most probably aligned along the dark fringes. This model explains as well the growth of a similar periodic structure with gold nanoparticles after UV exposure of the same glass doped with Au^{3+} ions.

The optical characterization of the periodic structure reveals narrow absorption bands in the optical absorption spectrum, whose presence is explained by the overlapping of the local fields between adjacent nanoparticles aligned along a line, spaced by only 20 nm. This indicates that silver nanoparticles with unique optical properties can be generated by our single step experimental technique. Pattern shapes could further be controlled varying the angle and polarization of the laser exposure. At the microscale, soda-lime glasses can be functionalized by approving the biological response resulting from an enhanced adhesion or adsorption of molecules, namely for SERS applications. We are currently working on the formation of a similar alignment with both gold and silver nanoparticles, which would broaden the wavelength range of these optical properties.

#197893 - $15.00 USD Received 17 Sep 2013; revised 6 Nov 2013; accepted 11 Nov 2013; published 16 Dec 2013